IEEE Photonics Journal
An IEEE Photonics Society Publication

Open Access

Broadband 4 × 4 Nonblocking Silicon Electrooptic Switches Based on Mach–Zehnder Interferometers

Volume 7, Number 1, February 2015

Liangjun Lu
Linjie Zhou, Member, IEEE
Zuxiang Li
Xinwan Li, Senior Member, IEEE
Jianping Chen

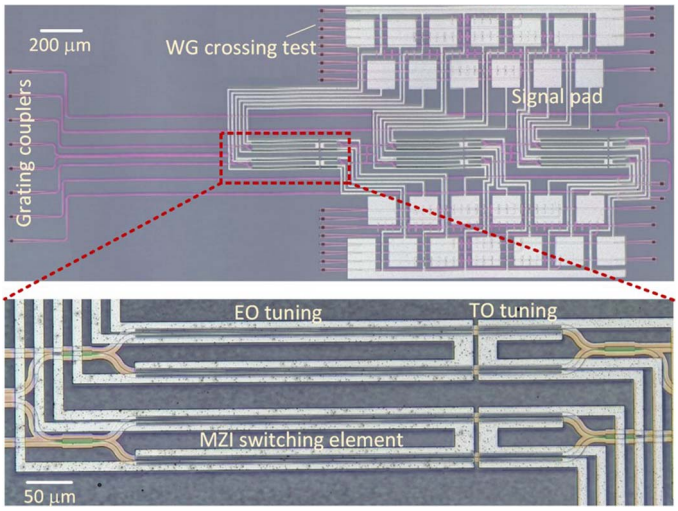

DOI: 10.1109/JPHOT.2015.2390195
1943-0655

Broadband 4 × 4 Nonblocking Silicon Electrooptic Switches Based on Mach–Zehnder Interferometers

Liangjun Lu, Linjie Zhou, *Member, IEEE*, Zuxiang Li, Xinwan Li, *Senior Member, IEEE*, and Jianping Chen

State Key Laboratory of Advanced Optical Communication Systems and Networks, Department of Electronic Engineering, Shanghai Jiao Tong University, Shanghai 200240, China

DOI: 10.1109/JPHOT.2015.2390195

Manuscript received December 2, 2014; revised January 4, 2015; accepted January 6, 2015. Date of publication January 8, 2015; date of current version January 26, 2015. This work was supported in part by the 973 Program under Grant ID2011CB301700, by the 863 Program under Grant 2013AA014402, by the National Natural Science Foundation of China under Grant 61127016 and Grant 61422508, and by the SRFDP of MOE under Grant 20130073130005. Corresponding author: L. Zhou (e-mail: ljzhou@sjtu.edu.cn).

Abstract: We report a broadband 4 × 4 nonblocking optical switch with Mach–Zehnder interferometers (MZIs) as switch elements on a silicon platform. Silicon resistive heaters are used for phase error correction of MZI arms with total thermooptic power consumption of 33.7 mW. Fast switching is enabled by p-i-n diodes, with average electrooptic tuning power of 14.3 mW for the 24 essential switching states as required for nonblocking routing. The average on-chip insertion loss is 5.8–7.7 dB and crosstalk better than −12 dB at wavelength of 1550 nm. Optical transmission experiments using a high-throughput 50 Gb/s quadrature phase-shift keying (QPSK) optical signal reveal that no significant deterioration is observed on constellation diagrams.

Index Terms: Silicon nanophotonics, integrated nanophotonic systems, optical interconnects.

1. Introduction

Optical switches, which route optical signals from multiple sources to multiple destinations, play a key role in both long-haul optical communications and short-reach optical interconnects [1], [2]. A variety of technologies has been developed to implement optical switches, such as micro-electro-mechanical systems (MEMS) [3], [4] and silica planar lightwave circuits (PLC) [5], [6]. The MEMS technology is well-suited for large-dimension optical switches with low wavelength and polarization dependence, and low crosstalk. The PLC-based optical switches are also feasible for scaling to large-port count, owing to their low insertion loss, planar integration, and easy coupling with optical fibers. However, both of them have the common disadvantages, such as large footprint, high power consumption, and low operation speed (in the millisecond to the microsecond range), which greatly limit their applications.

Silicon waveguides have the merits of sub-micrometer cross-section and low bending loss with the radii of only several micrometers. Meanwhile, the free carrier plasma dispersion effect (FCD) can provide a high tuning speed of up to 10's GHz. Besides, the fabrication is compatible with complementary metal-oxide-semiconductor (CMOS) technology, which lowers the cost and

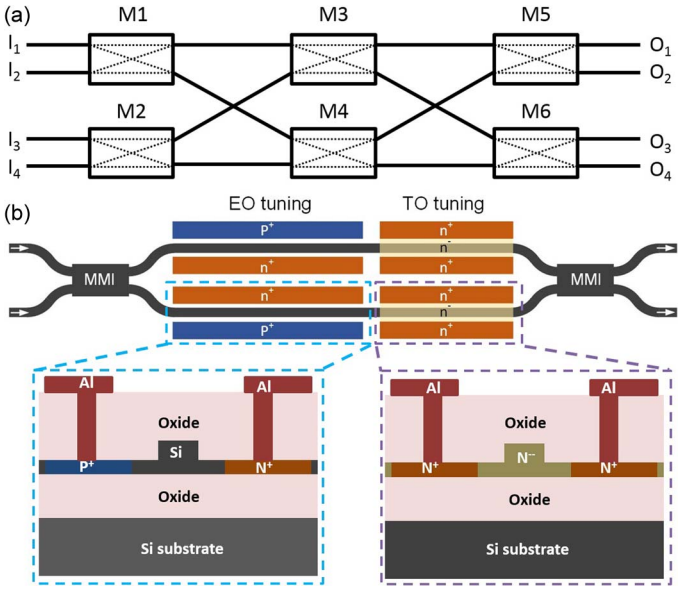

Fig. 1. (a) 4 × 4 Benes switch architecture. (b) Schematic view of the 2 × 2 MZI switch element. The insets show the cross-sections of the p-i-n diode and the silicon resistive heaters.

provides the possibility to combine microelectronic and photonic functionalities on one chip. In fact, silicon photonics technology has been developing rapidly and numerous passive and active optical components have been demonstrated on silicon-on-isolator (SOI) platforms [7]–[11], making it possible to realize optical switches based on silicon waveguide systems.

An N × N optical switch is usually formed by several 1 × 2 or 2 × 2 switch elements in a certain interconnect architecture. Single or coupled microring resonators (MRRs) can be utilized as the basic building blocks [12]–[17]. Previously, we demonstrated Mach-Zehnder interferometer (MZI) coupled MRRs to work as optical switches where electrical tuning is applied either to the MZI arm or to the MRRs [14], [15]. The MRR-based optical switches have the advantages of small footprint and low tuning power. However, their narrow optical bandwidth and high sensitivity to environmental temperature variation limit their practical applications. Comparing with the MRR, the MZI has a broader optical bandwidth and better tolerance to temperature variation [18]–[23], although the phase shift to change the switching state is much larger than the MRR.

In this paper, we report a broadband 4 × 4 non-blocking silicon electro-optic (EO) switch based on 2 × 2 MZI switch elements in a Benes architecture. The switch is composed of six MZIs, and each MZI is integrated with both EO and thermo-optic (TO) electrodes for fast switching and low loss phase error compensation, respectively. The average on-chip insertion loss of all 24 switching states is within 5.8 to 7.7 dB, with a routing path variation of ±2.3 dB. The measured worst crosstalk of the switch is −12 dB. The total TO tuning power is 33.7 mW and the average EO tuning power of the 4 × 4 switch in any given switching state is 14.3 mW. The switching functionality is verified by the transmission of a 50 Gb/s quadrature phase shift keying (QPSK) optical signal.

2. Device Design and Fabrication

Fig. 1(a) shows the schematic of the 4 × 4 Benes switch fabric. The Benes architecture, which is reconfigurably non-blocking, requires the least switch elements to obtain the full switching states and, hence, has the lowest insertion loss compared to Crossbar, Clos, Fat-Tree, Torus, and other architectures. A 4 × 4 Benes switch only needs three stages and six switch elements in total. As can be seen, waveguide crossings are necessary to construct the switch. In order to

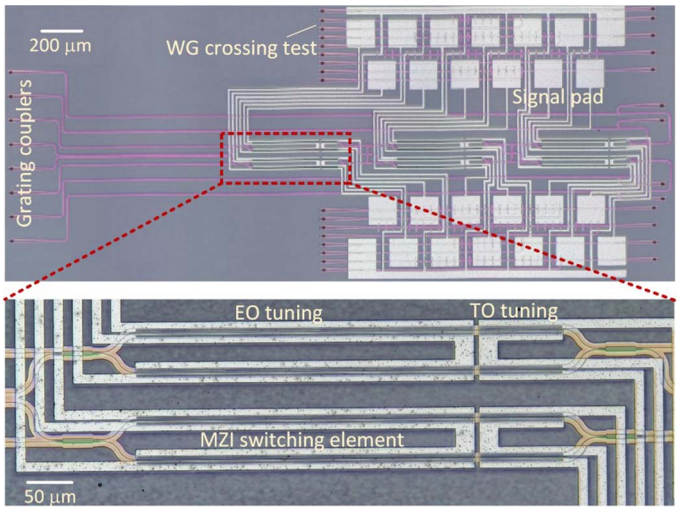

Fig. 2. Optical microscope image of the fabricated 4 × 4 switch. The inset shows the zoom-in view of the MZI switch element.

reduce the insertion loss and crosstalk of the waveguide crossing, we design 90°-cross 1 × 1 multimode interferometers (MMIs) based on the self-imaging principle for light to cross over the waveguide junction. The waveguide cross-section dimension is 0.5 μm (width) × 0.22 μm (height). The width and length of the MMIs are 1.15 and 4.77 μm, respectively. The MMI connection waveguides are broadened from 0.5 μm to 0.9 μm using linear tapers to reduce transmission loss.

Fig. 1(b) shows the switch element based on a 2 × 2 MZI. The MZI consists of two 2 × 2 MMIs linked by two arms with an equal length. Both of the two arms are integrated with p-i-n diodes for fast EO switching and silicon resistive heaters to correct fabrication induced phase errors [15], [24], as illustrated in the insets of Fig. 1(b). By changing the phase difference of the two arms from 0 to π, the MZI is switched from "cross" to "bar" state, which we defined as "0" and "1," respectively. There are totally $2^6 = 64$ combinations for the 4 × 4 switch, among which some are redundant. Only 24 permutations are needed for non-blocking operation.

The 4 × 4 switch is made up of silicon ridge waveguides with a slab thickness of 60 nm. The lengths of the p-i-n diodes and the silicon resistive heaters are 356 μm and 89 μm, respectively. The doping concentration of the highly doped p^+ and n^+ regions is $\sim 10^{20}$ cm^{-3}, separated from the waveguide edges by 0.8 μm to avoid free carrier absorption (FCA) loss. The resistive heater is made of lightly n^- doped silicon waveguide with a concentration of $\sim 8 \times 10^{16}$ cm^{-3} to reduce the resistance while maintaining low propagation loss. The device was fabricated using CMOS compatible processes.

Fig. 2 shows the optical microscope image of the fabricated device. Grating couplers with a period of 640 nm and a shallow etch depth of 70 nm are used for in- and out-coupling with a fiber array. The footprint of the 4 × 4 switch is 3.5 × 1.4 mm^2, including all the electrical pads and fiber array coupling region. It should be noted that the waveguides are elongated before terminated with grating couplers in order to leave enough space for fiber array coupling and wire bonding of electrical pads. In our design, we also add a directional coupler in each output waveguide so that light can be coupled out of the chip from both the left side (fiber array coupling) and the right side (individual fiber coupling) for easy testing. The directional coupler has a gap of 200 nm and a coupling length of 13 μm. The splitting loss for the fiber array end is about 6.2 dB around 1550 nm wavelength region based on finite-difference time-domain (FDTD) simulations. The signal pads were finally wire-bonded to a printed circuit board (PCB) for electrical tuning the silicon resistive heaters and the p-i-n diodes.

TABLE 1
Power Consumption of the Switch Elements

Switch elements	M1	M2	M3	M4	M5	M6
TO (mW)	6	7.2	4	7.6	8.1	0.81
EO (mW)	7.9	8.1	5.8	7.3	4.5	4.9

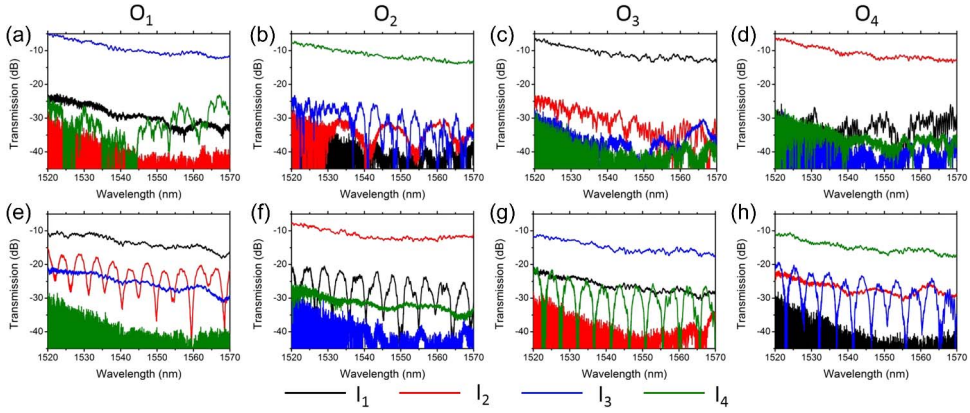

Fig. 3. Measured transmission spectra of the 4 × 4 switch when configured as (a)–(d) "000000" and (e)–(h) "111111" states.

3. Experimental Results

As there are phase errors for the as-fabricated devices, we first use TO tuning to correct the phase difference between MZI arms. After correction, the switch elements are all in the "cross" state which we refer to as the "000000" state. The TO power is fixed during the EO switching. We then change all switch elements from "cross" to "bar" states by tuning on the p-i-n diodes of the MZI bottom arms, so the 4 × 4 switch is configured to the "111111" state. The TO and EO power consumptions of the six switch elements are listed in Table 1. The total TO tuning power of the device is 33.7 mW. Because of the variations in the I-V characteristics of the p-i-n diodes, the EO power varies from 4.5 to 8.1 mW.

Fig. 3(a)–(d) show the measured transmission spectra of the 4 × 4 switch at the "000000" state. In each plot, the transmission spectra from the four input ports to one output port are recorded. The spectra are all normalized to a test waveguide to eliminate the effect of grating couplers. One can see that the input and output ports are mapped as $I_3 - O_1$, $I_4 - O_2$, $I_1 - O_3$, $I_2 - O_4$ with an on-chip insertion loss of around 10 dB. The loss comes from the switch elements, connection waveguides, waveguide crossings, and power splitters. The waveguide crossing loss is around 0.17 dB/junction at 1550 nm wavelength, extracted by linear fitting 10, 20, and 30 series-connected crossings. One might notice that the switch loss slightly increases with wavelength, it is because the directional couplers have a higher coupling ratio at a longer wavelength. The leaked power from the other three input ports become crosstalk to the main routing path. The worst crosstalk is around −15 dB. The crosstalk mainly results from the limited extinction ratio of the MZIs. Although we have corrected the phase errors in the MZI arms, the 2 × 2 MMIs in the MZI may not have an equal splitting ratio, which as a result cannot give 100% transmission in the "cross" state. The crosstalk can be further improved by optimizing the 2 × 2 MMIs. Fig. 3(e)–(h) show the transmission spectra of the "111111" state. As compared to the previous state, the insertion loss increases by ∼4 dB, and the crosstalk deteriorates to around −10 dB. The performance degradation is caused by the excess loss induced by FCA effect during the EO tuning. As a consequence, the optical power of the MZI two arms becomes

TABLE 2
Operation States and EO Tuning Power Consumption of the 4 × 4 Switch

No.	Switching states	O_1	O_2	O_3	O_4	EO tuning power (mW)
1	000000	I_3	I_4	I_1	I_2	0
2	001000	I_3	I_2	I_1	I_4	5.8
3	101000	I_3	I_1	I_2	I_4	13.7
4	000100	I_1	I_4	I_3	I_2	7.3
5	001100	I_1	I_2	I_3	I_4	13.1
6	000010	I_4	I_3	I_1	I_2	4.5
7	001010	I_2	I_3	I_1	I_4	10.3
8	000110	I_4	I_1	I_3	I_2	11.8
9	100110	I_4	I_2	I_3	I_1	19.7
10	001110	I_2	I_1	I_3	I_4	17.6
11	000001	I_3	I_4	I_2	I_1	4.9
12	001001	I_3	I_2	I_4	I_1	10.7
13	101001	I_3	I_1	I_4	I_2	18.6
14	000101	I_1	I_4	I_2	I_3	12.2
15	100101	I_2	I_4	I_1	I_3	20.1
16	010101	I_1	I_3	I_2	I_4	20.3
17	001101	I_1	I_2	I_4	I_3	18
18	000011	I_4	I_3	I_2	I_1	9.4
19	001011	I_2	I_3	I_4	I_1	15.2
20	101011	I_1	I_3	I_4	I_2	23.1
21	011011	I_2	I_4	I_3	I_1	23.3
22	000111	I_4	I_1	I_2	I_3	16.7
23	100111	I_4	I_2	I_1	I_3	24.6
24	001111	I_2	I_1	I_4	I_3	22.5

unbalanced, giving rise to a reduced extinction ratio and, hence, higher loss and crosstalk. It is also observable that some crosstalk spectra exhibit periodic oscillation patterns, e.g., $I_2 - O_1$, that is because of the interference of crosstalk paths with comparable optical power levels.

We also characterized the loss and crosstalk of all 64 switching states. Light at 1550 nm with transverse electric (TE) polarization is launched into one input port. A routing path from the input to a specific output is set up by setting the state of each MZI switch element upon tuning on the p-i-n diode with the power listed in Table 1. The transmitted optical power from this path is measured by a power meter. The ratio of the input light power to the measured output power is defined as the fiber-to-fiber insertion loss. Apart from the main path, the optical power is also partially coupled to the other three output ports, leading to crosstalk and noise. For each switching state, we measured the loss and crosstalk of all four paths. For non-blocking operation, only 24 switching states are essential. Table 2 lists the 24 switching states and their EO power consumptions. The total EO tuning power of all the six switch elements ranges from 0 to 24.6 mW over all 24 switching states. The average EO power consumption in any given switch configuration of the 4 × 4 switch is 14.3 mW. For the configurations that give the same state, we choose the one with the best performance.

Fig. 4(a) shows the measured fiber-to-fiber losses of the 24 states of the 4 × 4 switch. The coupling loss at 1550 nm is 7.5 dB per facet. The splitting loss of directional couplers is about 6.2 dB. The average on-chip insertion loss increases from 5.8 to 7.7 dB when the switch elements are changed from the “cross” state to the “bar” state due to FCA effect. The variation of on-chip insertion loss is ±2.3 dB.

Fig. 4(b) shows the crosstalk of all 24 switching states of the device. Here, the crosstalk of the input port m $(m \neq i)$ to the routing path $I_i - O_j$ $(i, j = 1, 2, 3, \text{and } 4)$ is defined as the ratio of the leaked output power $P_{out(m \to j)}$ to the output power $P_{out(i \to j)}$ [25]. Based on the definition, the leaked power for a specific routing path may come from three input ports; therefore, there are totally 12 crosstalk values for one switching state. The worst crosstalk of all the routing paths is −12 dB. As for practical use, all leaked power from the other three input ports

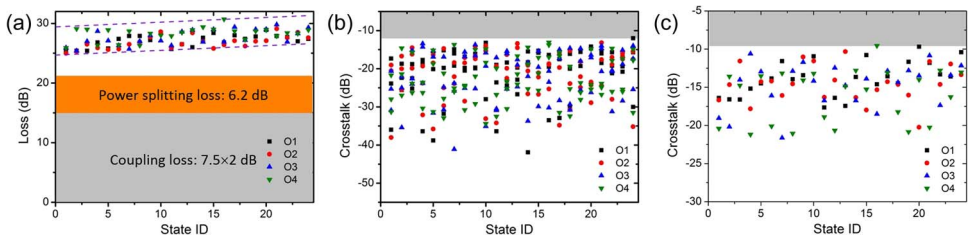

Fig. 4. (a) Fiber-to-fiber loss of each routing path. (b) Crosstalk to the four output ports from each noise path. (c) Accumulated crosstalk to the four output ports from all noise paths. All 24 switching states for non-blocking switching are measured.

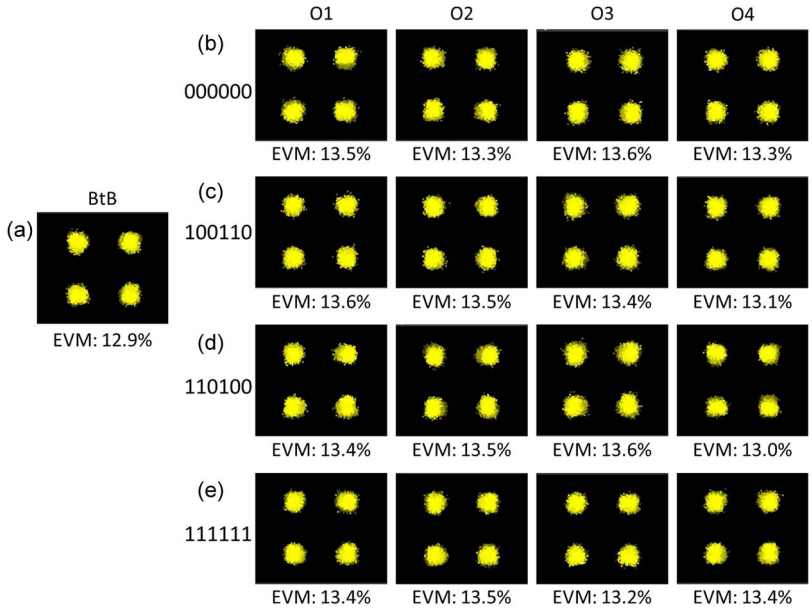

Fig. 5. Measured constellation diagrams of a QPSK signal. (a) Back-to-back transmission. (b) "000000" state. (c) "100110" state. (d) "110100" state. (e) "111111" state.

influences the main routing path. Hence, the accumulated crosstalk for any given routing path, defined as the summation of crosstalk contributed by all noise paths, is valuable assessment to the system performance when there are four simultaneously active input signals. Fig. 4(c) shows the accumulated crosstalk values at the four output ports for the 24 switching states, which are all better than -9.6 dB. It should be mentioned that the waveguide loss increases during EO tuning, and hence it is difficult to reduce the crosstalk of MZI switch elements to below -20 dB. In order to address this issue, more complicated switch units can be employed, for example, using double-gate 2×2 switch element made of 4 MZIs [26]. In this way, the crosstalk can be reduced to below -30 dB and the performance of our 4×4 switch can thus be further improved.

Next, we verify the switching functionality of the 4×4 switch by performing high-speed QPSK optical data transmission experiments. A continuous wave (CW) light at 1550 nm is generated by a tunable laser source, and is then modulated by a $LiNbO_3$ based IQ modulator to generate the QPSK signal. The modulator is driven by two 25 Gb/s $2^{31} - 1$ pseudo-random bit sequence (PRBS) radio frequency (RF) signals from a pulse-pattern generator (PPG); therefore, the bit rate of optical signal is 50 Gb/s. Before the optical signal is coupled to device, it is amplified by an erbium-doped fiber amplifier (EDFA) and is adjusted to TE polarization by a polarization controller (PC). The output optical signal from the chip is amplified by another EDFA to

compensate the loss of the device and followed by a band-pass filter to suppress the amplified spontaneous emission (ASE) noise from the EDFAs. A variable optical attenuator (VOA) is used to tune the optical power before it is received and analyzed by an optical modulation analyzer (Agilent, N4392A). The error-vector-magnitude (EVM) is obtained from the measured constellation diagrams.

We measured the data transmission of the "000000," "100110," "110100," and "111111" states. Fig. 5(a) shows the constellation diagram of the system back-to-back (BtB) transmission, with an EVM of 12.9%. The constellation diagrams of the four output ports under four switching states are illustrated in Fig. 5(b)–(e). The measured EVM are all smaller than 13.6%, which suggests the QPSK signal is degraded by less than 1% after passing through the device. Therefore, it illustrates that our device is capable of switching 50 Gb/s QPSK optical signal with high signal integrity, even though it has a relatively high loss.

4. Conclusion

We have demonstrated a silicon 4 $\times$ 4 non-blocking electro-optic switch based on a Benes architecture with MZIs as the switch elements. Phase errors in MZI arms are compensated by using silicon resistive heaters, with total TO power consumption of 33.7 mW. The switching operation is enabled by p-i-n diodes, with an average switching power of 14.3 mW in any given switch configuration. The measured transmission spectra show that the device is broadband with 5.8–7.7 dB average on-chip insertion loss for all 24 switching states at 1550 nm. The worst crosstalk of the switch at 1550 nm wavelength is -12 dB. Optical signal transmission measurements show that our device can switch 50 Gb/s QPSK signals with the EVM deteriorated by less than 1% comparing with BtB transmission.

References

[1] A. Shacham, K. Bergman, and L. P. Carloni, "Photonic networks-on-chip for future generations of chip multiprocessors," *IEEE Trans. Comput.*, vol. 57, no. 9, pp. 1246–1260, Sep. 2008.

[2] S. J. B. Yoo, "Optical packet and burst switching technologies for the future photonic Internet," *J. Lightw. Technol.*, no. 12, vol. 24, pp. 4468–4492, Dec. 2006.

[3] P. De Dobbelaere, K. Falta, S. Gloeckner, and S. Patra, "Digital MEMS for optical switching," *IEEE Commun. Mag.*, no. 3, vol. 40, pp. 88–95, Mar. 2002.

[4] M. Mizukami *et al.*, "128 $\times$ 128 three-dimensional MEMS optical switch module with simultaneous optical path connection for optical cross-connect systems," *Appl. Opt.*, vol. 50, no. 21, pp. 4037–4041, Jul. 2011.

[5] R. Kasahara *et al.*, "New structure of silica-based planar lightwave circuits for low-power thermooptic switch and its application to 8 $\times$ 8 optical matrix switch," *J. Lightw. Technol.*, vol. 20, no. 6, pp. 993–1000, Jun. 2002.

[6] T. Shibata *et al.*, "Silica-based waveguide-type 16 $\times$ 16 optical switch module incorporating driving circuits," *IEEE Photon. Technol. Lett.*, vol. 15, no. 9, pp. 1300–1302, Sep. 2003.

[7] L. Lu *et al.*, "CMOS-compatible temperature-independent tunable silicon optical lattice filters," *Opt. Exp.*, vol. 21, no. 8, pp. 9447–9456, Apr. 2013.

[8] Z. Haike *et al.*, "On-chip optical power monitor using periodically interleaved P-N junctions integrated on a silicon waveguide," *IEEE J. Sel. Topics Quantum Electron.*, vol. 20, no. 4, pp. 56–63, Jul. 2014.

[9] G. Binbin *et al.*, "CMOS compatible reconfigurable silicon photonic lattice filters using cascaded unit cells for RF-photonic processing," *IEEE J. Sel. Topics Quantum Electron.*, vol. 20, no. 4, Jul./Aug. 2014, Art. ID. 8202110.

[10] Y. Liu, J. M. Shainline, X. Zeng, and M. A. Popović, "Ultra-low-loss CMOS-compatible waveguide crossing arrays based on multimode Bloch waves and imaginary coupling," *Opt. Lett.*, vol. 39, no. 2, pp. 335–338, Jan. 2014.

[11] D. Liang and J. E. Bowers, "Recent progress in lasers on silicon," *Nat. Photon.*, vol. 4, pp. 511–517, Aug. 2010.

[12] N. Sherwood-Droz *et al.*, "Optical 4 $\times$ 4 hitless slicon router for optical networks-on-chip (NoC)," *Opt. Exp.*, vol. 16, no. 20, pp. 15915–15922, Sep. 2008.

[13] R. Ji *et al.*, "Five-port optical router for photonic networks-on-chip," *Opt. Exp.*, vol. 19, no. 21, pp. 20258–20268, Oct. 2011.

[14] L. Zhou and A. W. Poon, "Fano resonance-based electrically reconfigurable add-drop filters in silicon microring resonator-coupled Mach-Zehnder interferometers," *Opt. Lett.*, vol. 32, pp. 781–783, Apr. 2007.

[15] L. Lu, L. Zhou, X. Li, and J. Chen, "Low-power 2 $\times$ 2 silicon electro-optic switches based on double-ring assisted Mach-Zehnder interferometers," *Opt. Lett.*, vol. 39, no. 6, pp. 1633–1636, Mar. 2014.

[16] H. L. R. Lira, S. Manipatruni, and M. Lipson, "Broadband hitless silicon electro-optic switch for on-chip optical networks," *Opt. Exp.*, vol. 17, no. 25, pp. 22271–22280, Dec. 2009.

[17] P. Dasmahapatra, R. Stabile, A. Rohit, and K. A. Williams, "Crossbar switch matrix using fifth-order resonators," *Proc. IEEE 10th Int. Conf. GFP*, 2013, pp. 11–12.

[18] M. Yang *et al.*, "Non-blocking 4 × 4 electro-optic silicon switch for on-chip photonic networks," *Opt. Exp.*, vol. 19, no. 1, pp. 47–54, Jan. 2010.
[19] L. Chen and Y. K. Chen, "Compact, low-loss and low-power 8 × 8 broadband silicon optical switch," *Opt. Exp.*, vol. 20, no. 17, pp. 18977–18985, Aug. 2012.
[20] B. G. Lee *et al.*, "Monolithic silicon integration of scaled photonic switch fabrics, CMOS logic, and device driver circuits," *J. Lightw. Technol.*, vol. 32, no. 4, pp. 743–751, Feb. 2014.
[21] J. Xing *et al.*, "Nonblocking 4 × 4 silicon electro-optic switch matrix with push-pull drive," *Opt. Lett.*, vol. 38, no. 19, pp. 3926–3929, Oct. 2013.
[22] K. Suzuki *et al.*, "Ultra-compact 8 × 8 strictly-non-blocking Si-wire PILOSS switch," *Opt. Exp.*, vol. 22, no. 4, pp. 3887–94, Feb. 2014.
[23] M. R. Watts, J. Sun, C. DeRose, D. C. Trotter, R. W. Young, and G. N. Nielson, "Adiabatic thermo-optic Mach-Zehnder switch," *Opt. Lett.*, vol. 38, no. 4, pp. 733–735, Mar. 2013.
[24] L. Zhou, X. Zhang, L. Lu, and J. Chen, "Tunable Vernier microring optical filters with p-i-p type microheaters," *IEEE Photon. J.*, vol. 5, no. 4, Aug. 2013, Art. ID. 6601211.
[25] R. M. Jenkins *et al.*, "Novel 1 × N and N × N integrated optical switches using self-imaging multimode GaAs/AlGaAs waveguides," *Appl. Phys. Lett.*, vol. 64, no. 6, pp. 684–686, Feb. 1994.
[26] J. Xing, Z. Li, Y. Yu, and J. Yu, "Low cross-talk 2 × 2 silicon electro-optic switch matrix with a double-gate configuration," *Opt. Lett.*, vol. 38, no. 22, pp. 4774–4776, Nov. 2013.